ACS APPLIED MATERIALS & INTERFACES

Research Article

www.acsami.org

Modulation of Silica Nanoparticle Uptake into Human Osteoblast Cells by Variation of the Ratio of Amino and Sulfonate Surface Groups: Effects of Serum

Shakiba Shahabi,[†] Laura Treccani,*[,†] Ralf Dringen,[‡] and Kurosch Rezwan[†]

[†]Advanced Ceramics, University of Bremen, Am Biologischen Garten 2, 28359 Bremen, Germany

[‡]Centre for Biomolecular Interactions Bremen and Centre for Environmental Research and Sustainable Technology, Faculty 2 (Biology/Chemistry), University of Bremen, Leobener Strasse, NW2, 28359 Bremen, Germany

Supporting Information

ABSTRACT: To study the importance of the surface charge for cellular uptake of silica nanoparticles (NPs), we synthesized five different single- or multifunctionalized fluorescent silica NPs (FFSNPs) by introducing various ratios of amino and sulfonate groups into their surface. The zeta potential values of these FFSNPs were customized from highly positive to highly negative, while other physicochemical properties remained almost constant. Irrespective of the original surface charge, serum proteins adsorbed onto the surface, neutralized the zeta potential values, and prevented the aggregation of the tailor-made FFSNPs. Depending on the surface charge and on the absence or presence of serum, two opposite trends were found concerning the cellular uptake of FFSNPs. In the absence of serum, positively charged NPs were more strongly accumulated by human osteoblast (HOB) cells than negatively charged NPs. In contrast, in serum-containing medium, anionic FFSNPs were internalized by HOB cells more strongly, despite the similar size and surface charge of all types of protein-covered FFSNPs. Thus, at physiological condition, when the presence of proteins is inevitable, sulfonate-functionalized silica NPs are the favorite choice to achieve a desired high rate of NP internalization.

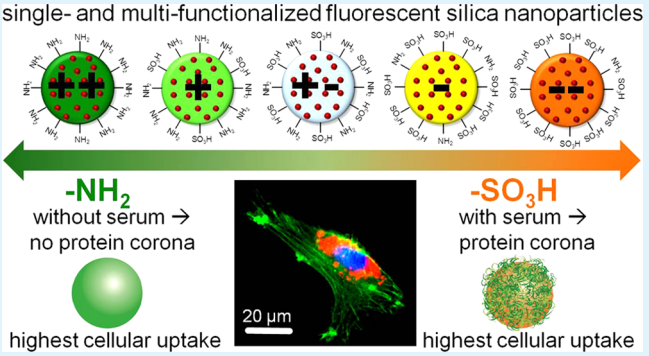

KEYWORDS: *cellular uptake, functionalization, osteoblast, protein corona, silica nanoparticle, surface charge*

1. INTRODUCTION

Silica nanoparticles (NPs) are a versatile, relevant system for various biomedical applications such as sensing,[1,2] imaging,[3,4] drug delivery,[5,6] DNA carriers,[7,8] and bioassays.[9] Due to their intrinsic features like high chemical stability, biocompatibility,[10] optical transparency,[11] and aqueous dispersibility,[12] silica NPs occupy a predominant position in biotechnology and medicine. Moreover, silica NPs can be easily functionalized,[13] and specific agents like peptides, proteins, and antibodies can be conjugated for cellular targeting.[14,15]

Despite many established bioconjugation strategies for targeting purposes with silica NPs, concerns regarding their clinical success have risen. Recently, it has been shown that the targeting capability and stability of bioconjugated NPs may disappear when they are placed in a biological environment.[16,17] The primary reason is the presence of a complex mixture of distinct proteins in the biological media.[18,19] Prior to cellular uptake, these proteins adsorb rapidly onto the surface of NPs, leading to the formation of a so-called "corona",[19−22] which may obscure specific recognition of bioligands on the NP surface and hamper their targeting applicability.[17,23] Indeed, at physiological conditions, biological systems are often exposed to NP−protein corona complexes, which differ significantly from bare NPs and define surface properties, aggregation rate, and hydrodynamic size of NPs.[19,24,25]

Protein corona formation is complex, inevitable, and unpredictable, but it is believed that NP surface properties can indirectly affect corona composition and evolution.[24] Surface functional groups are considered as the primary key factor to have a significant impact on protein binding[26,27] and subsequently also on biological behaviors such as tissue diffusion,[28] biodistribution,[29] and cellular uptake.[30,31]

The purpose of this study is to assess how surface functional groups on silica NP can be exploited to control cell responses in the presence and absence of serum proteins. We first report the synthesis of functionalized fluorescent silica NPs (FFSNPs) based on a reverse microemulsion method, which was followed by introducing amino and sulfonate groups at carefully chosen concentrations to generate single- or multifunctionalized silica NPs. Thereby, the surface charge was tuned successfully over a

Received: March 3, 2015
Accepted: June 1, 2015
Published: June 1, 2015

DOI: 10.1021/acsami.5b01900
ACS Appl. Mater. Interfaces 2015, 7, 13821−13833

Scheme 1. Schematic Illustration of the Synthesis and Simultaneous Functionalization of FFSNPs Using APTES and HSPSA (a) and of the Synthesized Particles Considering the Initial Molar Ratio of Functional Amino and Sulfonate Groups Used in the Synthesis (b) According to Table 1

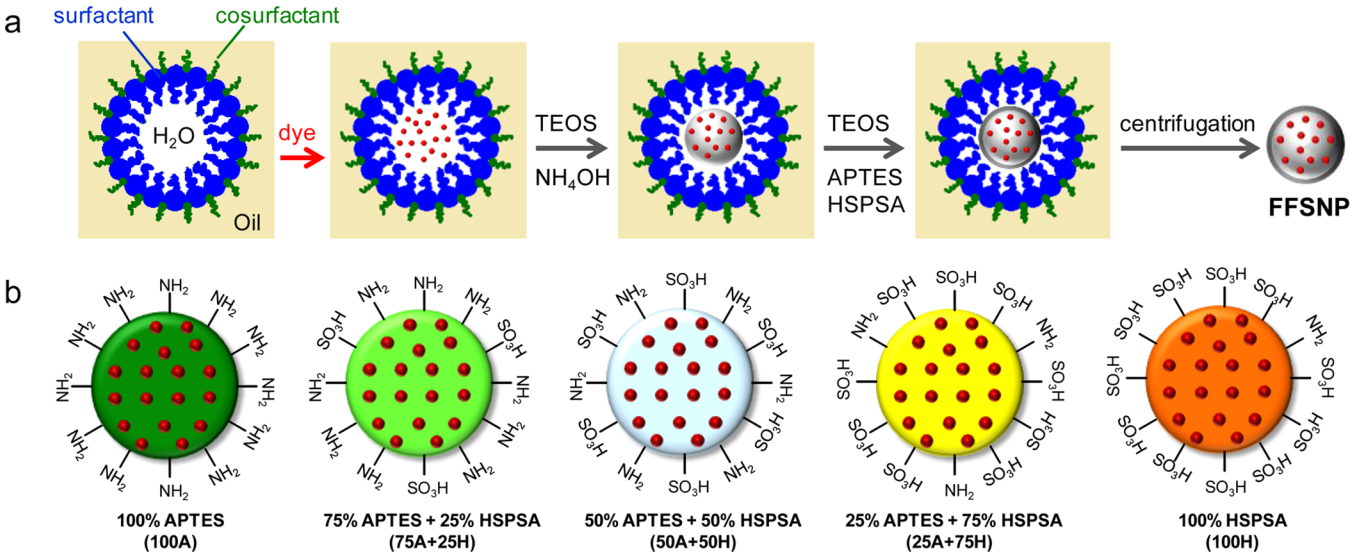

broad range from highly positive to highly negative, whereas other properties such as size, morphology, specific surface area, hydrophilicity, and fluorescence signal intensity remained approximately constant. This strategy enabled us to separate the effect of the net surface charge from the effects of the other mentioned physicochemical properties and to solely investigate the influence of surface charge on the interactions of the silica NPs with proteins and cells, without interference by other factors. The synthesized FFSNPs were characterized by scanning electron microscopy (SEM), scanning transmission electron microscopy (STEM), fluorescence microscopy, fluorescence spectroscopy, specific surface area (BET), adsorption capacity of polar and nonpolar gases, zeta potential, and dynamic light scattering (DLS). In order to understand how adsorbed serum proteins on FFSNPs affect the surface properties and the aggregation behavior, a combination of zeta potential and hydrodynamic diameter (D_H) measurements were performed in different media, including water, bovine serum albumin (BSA) containing water, and serum-supplemented and serum-free cell culture media under conditions identical to those used for cell experiments.

Our goal was to determine how the cellular uptake of FFSNPs would be affected by the surface charge and/or by the presence of attached serum proteins. To address these questions, the uptake and subcellular localization of cationic, neutral, and anionic FFSNPs within human osteoblast (HOB) cells under serum-containing and serum-free conditions were compared. The data obtained in these studies were linked to the investigation of the cytotoxic potential for the respective conditions.

2. MATERIALS AND METHODS

2.1. Materials. For particle synthesis, 1-hexanol (anhydrous, >99%, lot no. SHBC1238 V), Triton X-100 (lot no. BCBH1109 V), tetraethoxysilane (TEOS, >99%, lot no. BCBK1670 V), 25% aqueous ammonia solution (NH_4OH, lot no. SZBB0250 V), rhodamine B isothiocyanate (RBITC, mixed isomers, lot no. MKBJ9031 V), 3-aminopropyl-triethoxysilane (APTES, >98%, lot no. BCBH2173 V), and absolute ethanol (>98%, lot no. SZBB1570 V) were purchased from Sigma-Aldrich (Germany). 3-(Trihydroxysilyl)-1-propanesulfonic acid (HSPSA, 30−35% in H_2O, lot no. 1246512, ABCR, Germany), cyclohexane (anhydrous, 99.5%, batch no. 13B070516, VWR, Germany), bovine serum albumin (BSA, 99% protein, molecular weight 66.5 kDa, lot no. SLBG1645 V), and Pierce BCA protein assay (lot no. OC 185009, Thermo Scientific, Germany) were obtained from different suppliers as specified.

Cell culture tests were carried out on human osteoblast cells (HOB, lot no. 232R020412 obtained from Provitro (Germany)). Dulbecco/Vogt modified Eagle's minimal essential medium (DMEM, high glucose, lot no. 1206393), antibiotic-antimycotic (AB/AM, lot no. 1209917), Alexa Fluor 488 phalloidin (AF488, 2U/mL, lot no. 1151587), and LysoTracker (DND-22, lot no. 791512) from Invitrogen (Germany) and fetal calf serum (FCS, lot no. 010M3395), paraformaldehyde (PFA, lot no. 53260), phosphate buffered saline (PBS, lot no. SLBF5741 V), trypsin/ethylenediamine tetraacetic acid (EDTA) (0.25% trypsin, 0.02% EDTA, lot no. SLBG4376), Triton X-100 (lot no. MKBL5839 V), sodium chloride (NaCl, lot no. 038 K00451), 4′,6-diamidino-2-phenylindole (DAPI, 0.5 μg/mL, lot no. 1242642), chlorpromazine hydrochloride (lot no. 027M3145), wortmannin (lot no. 023M4072 V), nystatin (lot no. 020M13491), and dimethyl sulfoxide (DMSO, lot no. 055 K01033) from Sigma-Aldrich (Germany) were used. Water-soluble tetrazolium salt (WST-1) cell proliferation assay (lot no. 14310400, Roche Diagnostics GmbH, Germany) and lactate dehydrogenase (LDH) Pierce assay (lot no. OL17881450, Thermo Scientific, Germany) were purchased from the suppliers as specified. Double deionized water (ddH_2O) with a conductivity of <0.4 μS/cm was obtained from an ultrapure water system (Synergy, Millipore Corp., USA) and used as solvent for all solutions.

2.2. Preparation of Functionalized Silica NPs. FFSNPs were synthesized by a water-in-oil reverse microemulsion method according to refs 14 and 32 and as schematically shown in Scheme 1a. To covalently incorporate the dye in the silica matrix, RBITC was modified by inducing a reaction between the cyanate groups with the amino group of APTES. The RBITC derivative was prepared by adding APTES to RBITC previously dissolved in absolute ethanol (final concentration 1 mM) at the molar ratio of 1:1 (APTES/RBTIC). The mixtures was kept under darkness and stirred for 12 h at room temperature.

The microemulsion was formed by mixing 15 mL of cyclohexane, 3.6 mL of 1-hexanol, 3.54 mL of Triton X-100, and 1.1 mL of ddH_2O and stirred at room temperature for 10 min prior to the addition of 200 μL of the dye solution. After stirring for 30 min, 200 μL of tetraethoxysilane (TEOS) and 120 μL of ammonia solution (NH_4OH)

DOI: 10.1021/acsami.5b01900
ACS Appl. Mater. Interfaces 2015, 7, 13821−13833

Table 1. Physiochemical Properties of the Synthesized FFSNPs

sample	abbreviation	molar ratio of APTES	molar ratio of HSPSA	diameter (SEM [nm])	PDI	specific surface area [m^2/g]	water vapor adsorption [μmol/m^2]	*n*-heptane adsorption [μmol/m^2]
100% APTES	100A	1	0	58 ± 2	0.14 ± 0.03	48.7 ± 4.3	76.3 ± 5.5	40.9 ± 6.4
75% APTES + 25% HSPSA	75A + 25H	0.75	0.25	58 ± 2	0.2 ± 0.04	51.6 ± 2.6	77.7 ± 4.7	32.8 ± 4.4
50% APTES + 50% HSPSA	50A + 50H	0.5	0.5	58 ± 2	0.23 ± 0.03	56.4 ± 2.4	70 ± 3.6	39.8 ± 6.3
25% APTES + 75% HSPSA	25A + 75H	0.25	0.75	58 ± 2	0.17 ± 0.04	54.9 ± 1.7	69.9 ± 5.7	33.3 ± 5.6
100% HSPSA	100H	0	1	58 ± 2	0.19 ± 0.01	57.7 ± 3.1	64.2 ± 7.2	36.1 ± 4

were added to initiate the hydrolysis and condensation. The reaction mixture was stirred for 24 h at room temperature before introducing amino or/and sulfonate groups to functionalize the NPs. As illustrated in Scheme 1b and Table 1, for single-functionalized NPs (100A and 100H), 0.11 mM 3-aminopropyl-triethoxysilane (APTES) or 3-(trihydroxysilyl)-1-propanesulfonic acid (HSPSA) was used, whereas the other three NPs (75A + 25H, 50A + 50H, and 25A + 75H) were mixed-functionalized with the appropriate molar ratios of APTES to HSPSA. The lowest possible amount of both reagents for functionalization was optimized to tune the zeta potential of the final NPs but keeping the other properties almost constant, as later discussed. After 24 h, stirring the reaction was stopped by addition of acetone. Afterward, FFSNPs were collected by centrifugation and washed several times with absolute ethanol and ddH_2O to remove any unreacted chemicals and free dye molecules.

2.3. Particle Characterization. For characterization, dispersions of FFSNPs were obtained by ultrasonication using an ultrasound horn (Sonifier 450, Branson, Germany) at an ultrasound frequency of 20 kHz, with two ultrasound pulses of 150 W/s for 15 min. Scanning electron microscopy (SEM) images of FFSNPs were taken with a Supra 40 (Carl Zeiss, Germany) operated at 2.00 kV. No conductive coating was deposited on the particles. STEM images were recorded using a Titan 80−300 ST microscope (FEI, Eindhoven, The Netherlands). FFSNPs were deposited onto a carbon-coated copper grid (PLANO GmbH, Wetzlar, Germany) by carefully shaking to leave only a small deposit.

Fluorescence spectra of FFSNPs aqueous suspensions (0.05 vol %) were recorded using a LS 50 spectrometer (PerkinElmer, Germany). The slit widths for excitation and emission were 10 and 5 nm, respectively. Fluorescence microscopy of FFSNPs and cells after in vitro tests was performed with an AX-10 fluorescence microscope (Zeiss, Germany) using three fluorescence channels, including FS02 for 4′,6-diamidino-2-phenylindole (DAPI) (λ_{ex}: 300−400 nm; λ_{em}: >420 nm), FS09 for Alexa Fluor 488 phalloidin (AF488) (λ_{ex}: 450−490 nm; λ_{em}: >515 nm), and FS15 (λ_{ex}: 535−558 nm; λ_{em}: >590 nm) for rhodamine B isothiocyanate (RBITC).

Nitrogen adsorption on the surface was measured to calculate the specific surface area according to the method of Brunauer et al. (BET).[33] Measurement of the adsorption isotherms as well as calculation of the specific surface areas was performed with a BELSORP-mini (BEL Japan Inc., Osaka, Japan) and the accompanying software (BELMaster). Samples were vacuum-dried at <0.5 mbar and 120 °C for 2 h prior to measurement.

The hydrophilic/hydrophobic properties of the synthesized FFSNPs were determined by volumetric vapor adsorption studies of polar (water) and nonpolar (*n*-heptane) gases at a temperature of 22 °C in a BELSORP 18-3 (Bel Inc., Japan). Prior to the adsorption measurements, all NPs were outgassed for 24 h at 100 °C under argon.

Zeta potential measurements of FFSNPs dispersions were carried out in different media, including ddH_2O, 1% bovine serum albumin (BSA) dissolved in ddH_2O (H_2O + BSA (1%)), Dulbecco/Vogt modified Eagle's minimal essential medium (DMEM) containing 1% antibiotic-antimycotic (AB/AM) (DMEM + AB/AM (1%)), and DMEM supplemented with 10% fetal calf serum (FCS) and 1% AB/AM (DMEM + FCS (10%) + AB/AM (1%)). The dispersions of FFSNPs (5×10^{-4} vol %) were prepared, and their zeta potential was determined 0.5 h after preparation using the Delsa Nano C photospectrometer (Beckman Coulter, Brea, CA). The average values and standard deviations given were obtained from three replicates.

For measurement of BSA adsorption, the dispersions of FFSNPs in H_2O + BSA (1%) were incubated at 37 °C for 0.5, 2, 4, or 6 h. To quantify the amount of adsorbed BSA after each incubation time interval, FFSNP−protein conjugates were separated by centrifugation for 10 min at 20 000*g* and the supernatants were centrifuged again for 10 min at 20 000*g*. The concentrations of BSA in the supernatants were determined with the BCA assay according to the supplier's instructions and using a multiscan GO spectrophotometer (Thermo Scientific, Finland). The averages and standard deviations of data from three independent measurements are given.

The particle sizes of the five synthesized FFSNPs were measured using DLS with the Delsa Nano C photospectrometer. To determine the effects of surface charge and presence of serum proteins on colloidal stability, triplicate measurements of hydrodynamic size were acquired from the dispersions of FFSNPs (5×10^{-4} vol %) in H_2O, H_2O + BSA (1%), DMEM + AB/AM (1%), and DMEM + FCS (10%) + AB/AM (1%) 0.5, 2, 4, or 6 h after preparation. The polydispersity index (PDI) of the colloidal particles in the different media was calculated on the basis of the cumulative analysis of the light scattering data, which was performed automatically by the DLS instrument. The average sizes, d_{50}, and standard deviations were obtained from three independent measurements. The four time points were selected to allow comparison to the respective conditions of in vitro experiments.

2.4. Cell Culture Experiments. *2.4.1. Cell Culturing.* Cell culture experiments were performed with HOB cells as described in Holthaus et al.[34] Briefly, cells (4th passage) were cultured in DMEM supplemented with 10% heat-inactivated FCS and 1% AB/AM in an incubator (C200, Labotect Labor-Technik-Göttingen, Germany) at 37 °C with 10% CO_2 and 95% relative humidity (RH). Cells were cultured in cell culture flasks (75 cm^2) for up for 1 week, and the medium was renewed every 2 days. HOBs were trypsinized and dispersed in either DMEM + AB/AM (1%) or DMEM + FCS (10%) + AB/AM (1%) for cell experiments without and with serum, respectively. HOBs were seeded at a density of 3×10^4 cells in 800 μL of medium onto 15 mmØ Thermanox coverslips (NUNC, Fischer Scientific, Germany) placed in wells of 24-well polystyrene multidishes (NUNC, Fischer Scientific, Germany) and incubated at 37 °C with 10% CO_2 and 95% RH. After 1 h, 100 μL dispersions containing 0.5 and 1 mg FFSNPs/mL in DMEM + AB/AM (1%) or DMEM + FCS (10%) + AB/AM (1%) were freshly prepared and added to the cell culture medium in each well to establish a final particle concentration of 50 and 100 μg/mL, respectively, and cells were incubated for 0.5, 2, 4, or 6 h. As control, HOB cells were incubated in the absence of FFSNPs. Incubations for longer than 6 h were not performed, as the cell viability for the serum-free incubation conditions were compromised under those conditions even in the absence of FFSNPs (data not shown).

2.4.2. Cell Staining and Imaging. After exposure to FFSNPs, the HOB cells were rinsed twice with phosphate buffered saline (PBS) buffer to remove noninternalized NPs, fixed with paraformaldehyde (PFA), and fluorescently stained with DAPI for the cell nuclei and with AF488 for actin cytoskeletons. FFSNPs uptake and internalization within the cells were analyzed using an AX-10 fluorescence microscope (Zeiss, Germany).

Cellular localization of FFSNPs in lysosomes was investigated by coincubation with LysoTracker. To avoid possible autofluorescence of

DOI: 10.1021/acsami.5b01900
ACS Appl. Mater. Interfaces 2015, 7, 13821−13833

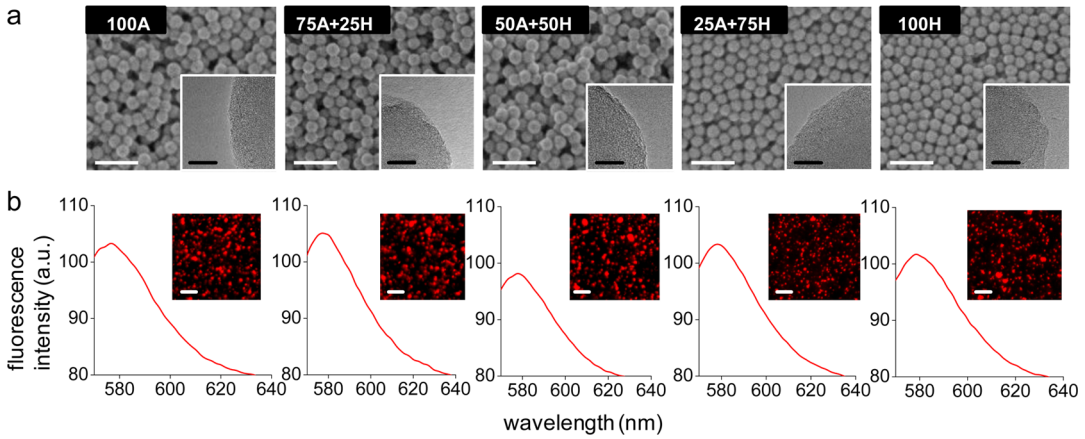

Figure 1. SEM and STEM (insets) micrographs of FFSNPs (a) and fluorescence emission spectra of FFSNPs aqueous suspensions at 550 nm excitation and fluorescence microscopy micrographs (b). Scale bars are 200 nm, 10 nm, and 20 μm in all SEM, STEM, and fluorescence microscopy images, respectively.

Thermanox coverslips in the lysosomal colocalization experiments, HOB cells were cultured on glass coverslips (lot. no. 0983, VWR, Germany). As explained above, the cells were exposed to the FFSNPs at a concentration of 50 or 100 μg/mL, followed by a 1 h incubation with LysoTracker (75 nM) in the given incubation media. Thereafter, the cells were washed twice with PBS and fixed with PFA. Cell actin cytoskeleton was stained with AF488. The applied LysoTracker is a blue fluorescent dye that stains the acidic lysosomes. Hence, cellular colocalization of the RBITC labeled silica NPs (red fluoresce) with LysoTracker will yield a magenta overlap in merged images.

2.4.3. Quantification of Cellular Uptake of FFSNPs. To estimate cellular association of FFSNPs, after each sampling point, the HOBs were trypsinized and washed with PBS (three times with a centrifugation each time at 600*g* for 5 min). Subsequently, the cell pellet was resuspended in PBS and analyzed by fluorimetry in black well plates (Greiner Bio-One, Germany) using a microplate reader (Chameleon, HIDEX, Turku, Finland) at the excitation wavelength of 544 and emission of 590 nm. Data are expressed as fluorescence intensity units after subtracting background (cells without NPs) and normalized to the fluorescence intensity of the applied FFSNPs dispersions.

2.4.4. Determination of Cell Viability. Cell viability was evaluated using a colorimetric water-soluble tetrazolium salt (WST-1) cell proliferation assay. After a given incubation period, 100 μL of WST-1 cell proliferation reagent was added to the culture wells and the cells were incubated for 2 h at 37 °C with 10% CO_2 and 95% RH. Thereafter, the cell medium was harvested and centrifuged at 20 000*g* for 5 min to remove the FFSNPs. Formazan produced and released by living cells was quantified spectrometrically using a multiscan GO spectrophotometer (Thermo Scientific, Finland) at 450 nm with a reference wavelength of 650 nm. An identical volume of culture medium and reagent WST-1, which had not been in contact with the cells, was used in the experiment as a blank.

The cellular and extracellular activity of the cytosolic enzyme lactate dehydrogenase (LDH) was quantified using the Pierce assay according to the supplier's instruction. After each time interval, the media were collected from each well and centrifuged at 20 000*g* for 5 min to remove the NPs before measurement of extracellular LDH. For quantification of cellular LDH, the cells were rinsed with PBS buffer, detached with trypsin/ethylenediamine tetraacetic acid (EDTA) solution, and centrifuged at 600*g* for 10 min to separate the cell pellet from the supernatant. Afterward, the lysis buffer (1% Triton X-100 in 0.9% NaCl) was added to the cell pellet and mixed until a clear solution was obtained. 50 μL of media or cell lysates was used in the assay, and the absorbance at 490 nm with a reference wavelength of 680 nm was measured using the above-mentioned spectrophotometer. LDH release as indicator for damaged cells was calculated by dividing the measured amount of extracellular LDH activity by the total LDH activity (medium plus lysate).

2.4.5. Inhibition of Endocytosis. In order to discriminate between possible endocytosis pathways of FFSNPs in HOB cells, their uptake was quantified in the presence or absence of the endocytosis inhibitors, chlorpromazine (30 μM), wortmannin (300 nM), or nystatin (10 μM), after 2 h of exposure. In addition, cells were incubated at 4 °C with FFSNPs for 2 h to study the possible temperature-dependent inhibition of cellular FFSNP accumulation. Subsequently, the cellular content of particles was analyzed by fluorimetry of cell pellets as described above. The data are given as a percentage of the respective FFSNP-treated cells at 37 °C, with DMSO and without inhibitors (control).

2.5. Statistical Analysis. The results assessed by BCA, WST-1, and LDH assays as well as the values derived from cellular uptake experiments are given as mean ± standard deviation of three independently performed experiments. The statistical analysis was performed using the software Minitab 16 (Minitab Inc., Pennsylvania). The data were subjected to one-way analysis of variance (ANOVA) followed by Dunnett's method for multiple comparisons. *p*-values below 0.05 were considered to be statistically significant.

3. RESULTS

Table 1 summarizes the properties of the synthesized FFSNPs and lists the molar ratios of amino and sulfonate groups, diameter defined by SEM micrographs, PDI obtained by DLS, and specific surface area measured by BET as well as the adsorption of water vapor and *n*-heptane. The values determined for the specific surface area differ only slightly between the type of surface functionalization as the lowest and highest specific surface areas were measured for 100A (48.7 ± 3.3 m^2/g) and for 100H (57.7 ± 3.1 m^2/g), respectively.

To quantify the effect of surface functionalization with various ratios of amino and sulfonate groups on the hydrophilic/hydrophobic properties of silica, the adsorption isotherms of polar water vapor and nonpolar *n*-heptane on the FFSNPs were measured (Table 1). No significant difference between the results obtained for the five FFSNPs was observed, suggesting the similar hydrophilicity of the synthesized FFSNPs, irrespective of the ratio of the introduced amino and sulfonate functional groups.

This table lists the five types of FFSNPs analyzed with their short notation, the molar ratios of APTES and HSPSA used for the synthesis, the diameter assessed from SEM images, the polydispersity index (PDI) obtained from DLS measurements

DOI: 10.1021/acsami.5b01900
ACS Appl. Mater. Interfaces 2015, 7, 13821−13833

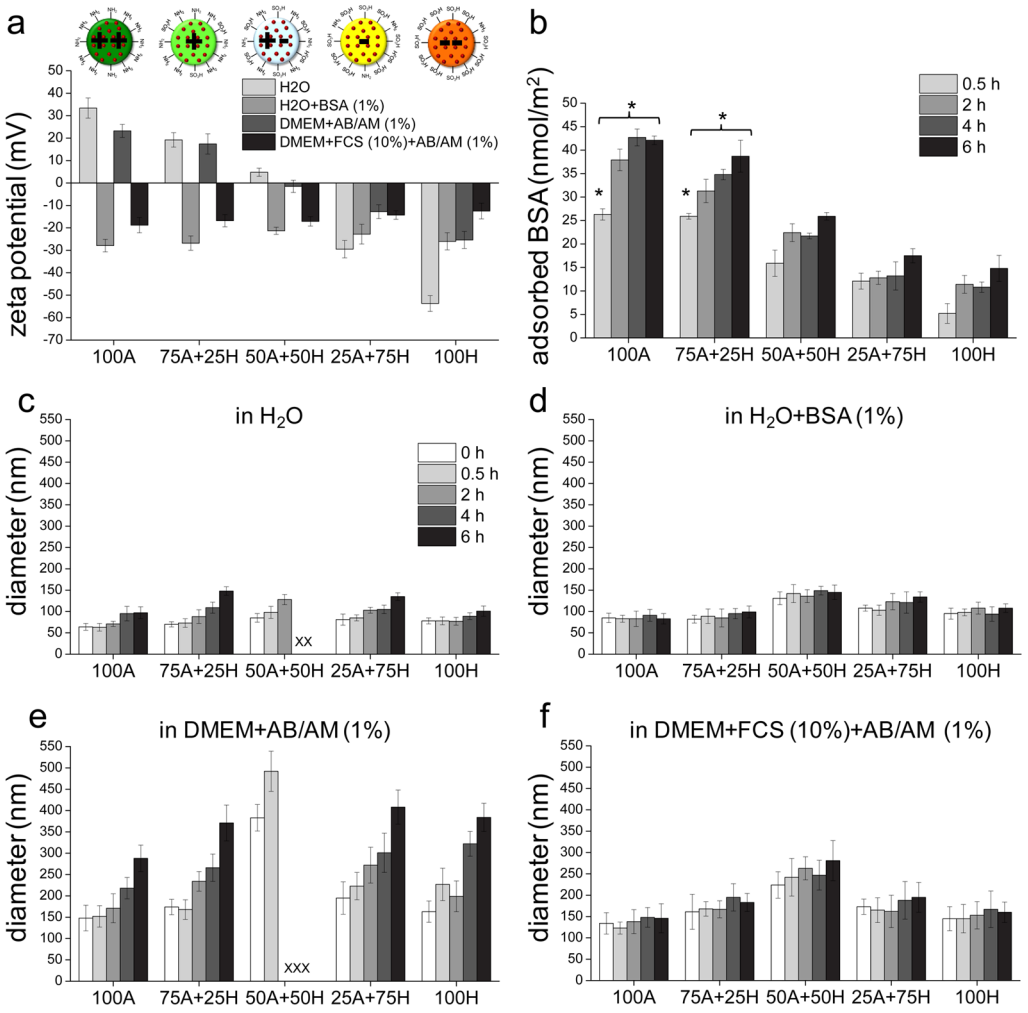

Figure 2. Physicochemical properties of FFSNPs in different media. The zeta potential (a) of FFSNPs in the given media was measured 0.5 h after preparation. Panel (b) shows the amount of adsorbed BSA (normalized to the specific surface area) determined for FFSNPs which had been dispersed in H_2O containing 1% BSA for 0.5, 2, 4, or 6 h at 37 °C. Panels (c–f) show the average hydrodynamic diameters of FFSNPs as a function of time in the indicated media, demonstrating colloidal stability or instability. In (b), asterisks (*) show a significant difference in BSA adsorption ($p < 0.05$) for each particle between different incubation times. Sedimentation or severe aggregation of FFSNPs, corresponding to D_H larger than 550 nm or PDI > 0.3, are indicated by X in panels (c, e).

in H_2O, and the specific surface area as well as the adsorption capacity of water vapor and *n*-heptane. The data represent means ± SD of three independent measurements.

SEM and STEM analysis revealed that all types of FFSNPs synthesized are of spherical shape and show a narrow size distribution (Figure 1a) with a mean diameter of 58 nm (Table 1). The fluorescent emission spectra of the FFSNPs were measured at the excitation wavelength of RBITC (550 nm) and are shown in Figure 1b. All FFSNPs presented a well distinct fluorescence signal at the emission wavelength of RBITC. This was further confirmed by fluorescence microscopy, which indicated that all FFSNPs feature bright fluorescence.

The zeta potential values of the synthesized FFSNPs in aqueous dispersions varied greatly over a broad range from 33.4 ± 4.5 to −53.7 ± 3.5 mV (Figure 2a). By variation of the surface charge via single- and multifunctionalization, two cationic (100A and 75A + 25H), one almost neutral (50A + 50H), and two anionic silica NPs (25A + 75H and 100H) were synthesized. An analogous variation of surface charge was observed for the FFSNP dispersions prepared in DMEM + AB/AM (1%) which ranged between 23.2 ± 2.9 and −25.4 ± 3.8 mV. DMEM supplemented with 10% FCS is commonly used as a cell culture medium for in vitro studies. Therefore, the zeta potentials of FFSNPs were also measured for dispersions in DMEM + FCS (10%) + AB/AM (1%). In serum-containing medium, all the FFSNPs had acquired a negatively charged surface (−12.5 ± 3.5 to −18.8 ± 3.4 mV). Due to the complexity of serum-supplemented medium, we selected BSA as a model protein and measured zeta potential of FFSNPs in H_2O + BSA (1%), as BSA is the most abundant protein found in plasma and in NP protein corona.[35,36] The concentration of BSA (1%) was chosen, as it is equivalent to the total protein concentration present in the 10% FCS.[37] Negative zeta potential values (−21.3 ± 1.6 to −27.9 ± 2.8 mV) were obtained from FFSNP dispersions prepared in H_2O + BSA (1%), regardless of the original surface charges of the NPs.

The amount of BSA adsorbed on the FFSNPs was measured after incubation for 0.5, 2, 4, or 6 h at 37 °C. For all incubation times, the two cationic FFSNPs (100A and 75A + 25H) showed higher BSA adsorption compared to the particles with neutral and negative charges (Figure 2b). For the cationic FFSNPs, a significant increase of protein adsorption ($p < 0.05$)

DOI: 10.1021/acsami.5b01900
ACS Appl. Mater. Interfaces 2015, 7, 13821−13833

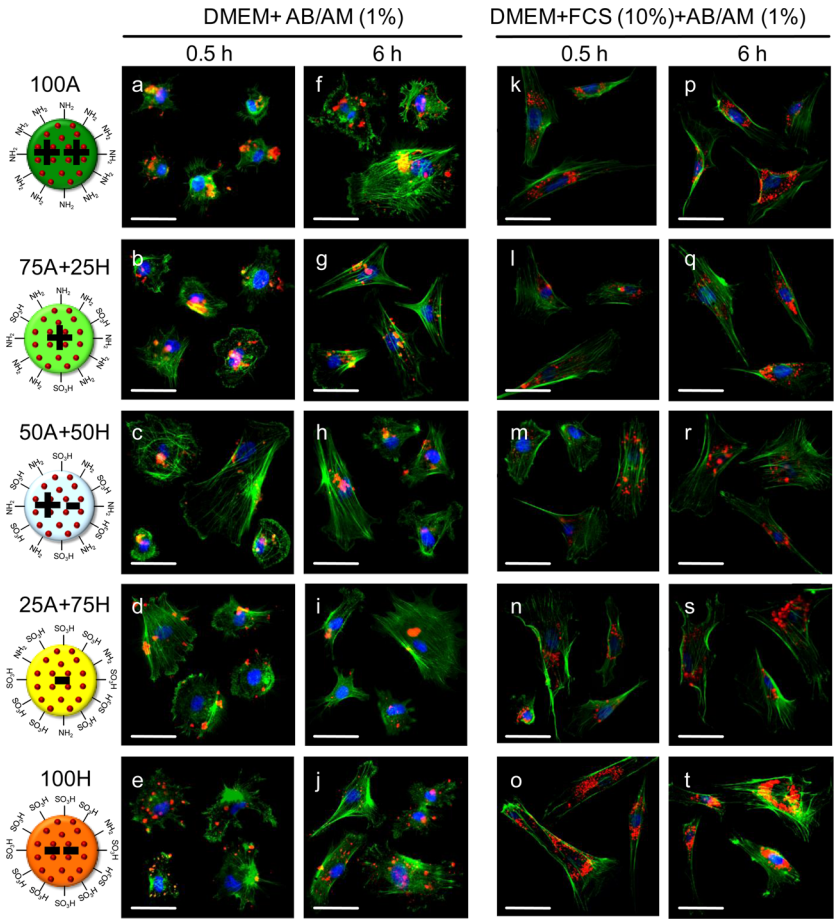

Figure 3. Fluorescence microscopy micrographs of HOB cells incubated without (a–j) or with (k–t) FCS for 0.5 or 6 h at 37 °C with 100 μg/mL FFSNPs, revealing cellular uptake and intracellular localization of the particles. In all images, green, blue, and red fluorescence indicates the actin cytoskeleton, the nuclei, and FFSNPs, respectively. Scale bars: 50 μm.

was found after 2 h compared to the 0.5 h incubation period, but thereafter, the amount of adsorbed BSA remained almost constant. In contrast, for neutral and anionic NPs, the amount of adsorbed protein had reached almost maximal values already after 0.5 h and these values did not significantly change during longer incubation (Figure 2b).

The size distributions of FFSNP in freshly prepared aqueous dispersions, as obtained by DLS, are shown in Figure S1 (Supporting Information). The colloidal stability of FFSNPs during incubation in different media was investigated by monitoring the changes in their hydrodynamic diameter (D_H) upon incubation in the different media, including H_2O, H_2O + BSA (1%), DMEM + AB/AM (1%), and DMEM + FCS (10%) + AB/AM (1%) and at different time points (0, 0.5, 2, 4, or 6 h after preparation) as shown in Figure 2c–f. FFSNPs dispersions showing sedimentation or severe aggregation, corresponding to D_H larger than 550 nm or PDI higher than 0.3, were not quantified and are indicated by X (Figure 2c,e). For aqueous suspensions of charged FFSNPs, including 100A, 75A + 25H, 25A + 75H, and 100H, a slight increase of D_H was observed with increasing incubation time. In contrast, neutral particles (50A + 50H) showed significant aggregation after 2 h in water (Figure 2c). All five FFSNPs were colloidally stable in H_2O + BSA (1%) and DMEM + FCS (10%) + AB/AM (1%) during an incubation time of up to 6 h (Figure 2d,f). Nevertheless, for all FFSNPs, an increase of D_H was observed in DMEM + AB/AM (1%) which was particularly strong for neutral FFSNP (50A + 50H), and severe aggregation and sedimentation were already shown after 0.5 h of incubation (Figure 2e).

The uptake of FFSNPs with various surface charges into HOB cells was studied in the absence and presence of serum. Particle internalization in HOBs was characterized by fluorescence microscopy. Results obtained after 0.5 or 6 h of exposure to the FFSNPs at the final concentration of 100 μg/mL are presented in Figure 3. In all fluorescence microscopy micrographs, actin cytoskeletons (green) and nuclei (blue) were stained with AF 488 and DAPI, respectively. RBITC labeled FFSNPs are visible with their typical red fluorescence. Particle uptake into HOBs was observed for both serum-free and serum-containing incubation media for all types of FFSNPs investigated (Figure 3). Fluorescence microscopic inspection of the treated cultures revealed that for all conditions investigated more than 90% of the cells contained FFSNPs (data not shown).

To investigate a potential intracellular colocalization of FFSNPs with lysosmes, after exposure with FFSNPs for 0.5, 2, 4, or 6 h, the lysosomes were specifically stained with LysoTracker. Fluorescence microscopy for FFSNPs, actin cytoskeletons, and lysosomal components was performed with appropriate specific channels, which detect the emitted fluorescence light in the red, green, and blue colors, respectively. Due to similarities in the results for the different incubation periods investigated, only representative fluorescence microscopy images for 6 h incubations of the HOBs with

DOI: 10.1021/acsami.5b01900
ACS Appl. Mater. Interfaces 2015, 7, 13821–13833

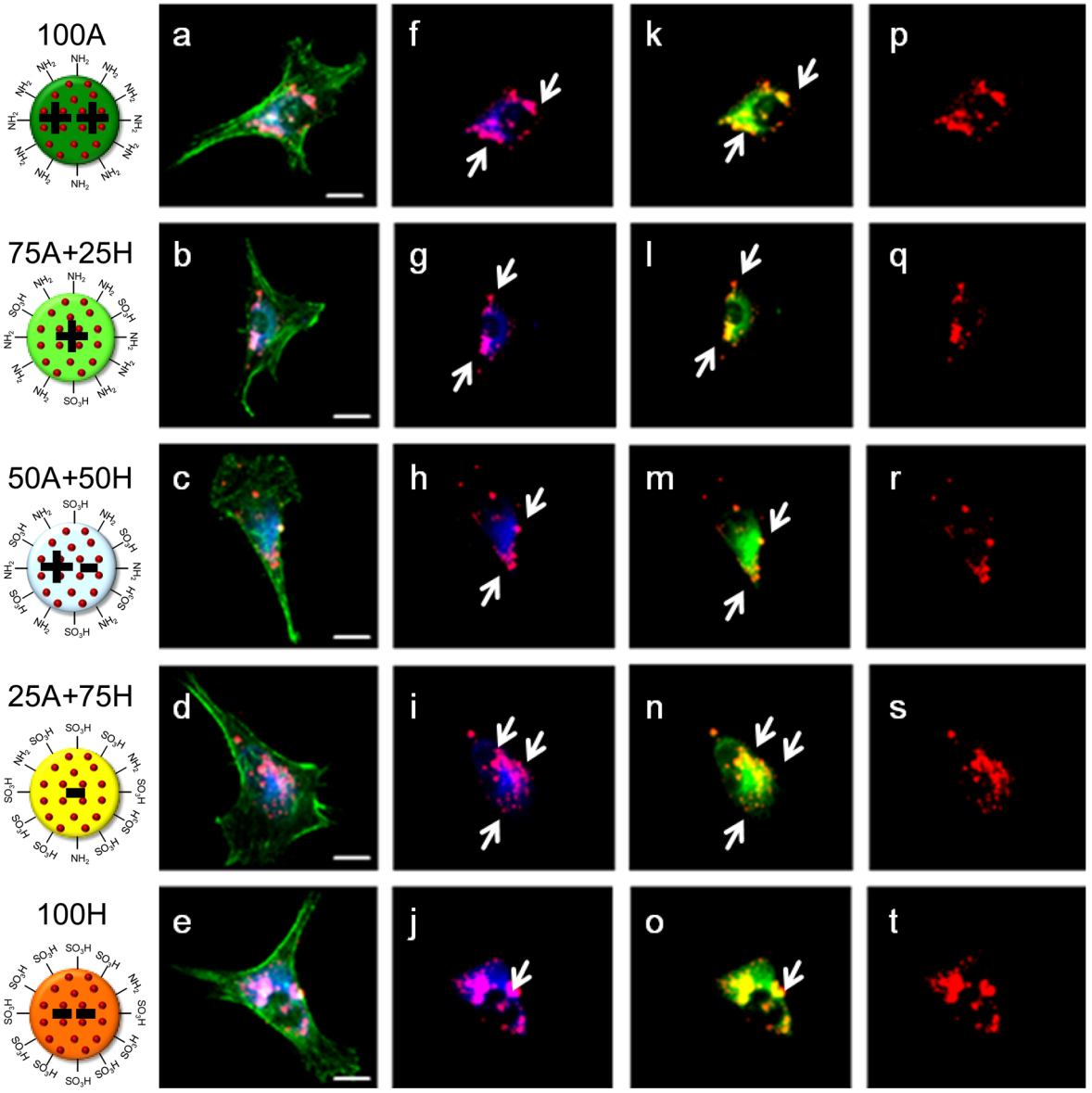

Figure 4. Colocalization of FFSNPs (100 μg/mL) and lysosome after a 6 h incubation in DMEM + FCS (10%) + AB/AM (1%) at 37 °C. The images in panels (a–e) represent the merged fluorescence signals recorded in the green (cytoskeleton), blue (LysoTracker), and red (FFSNPs) channels. The micrographs in panels (f–o) show the overlay of LysoTracker and FFSNPs. In (f–j), the LysoTracker is shown with its original blue fluorescence; therefore, the overlay with FFSNPs is indicated by a magenta color, whereas in panels (k–o), the LysoTracker is presented with a pseudo green color, in order to demonstrate the overlapping with red NPs, which is observable as a yellow color. The overlays of cellular fluorescences for LysoTracker and FFSNPs, as indicated by white arrows, demonstrate the accumulation of FFSNPs inside the endolysosomal compartment. The images in panels (p–t) present the fluorescence signal from the FFSNPs in the single red channel. Scale bars: 100 μm.

FFSNPs (100 μg/mL) in DMEM + FCS (10%) + AB/AM (1%) are presented (Figure 4). Panels (a–e) show merged images of signals from the three fluorescence microscope channels. The micrographs in panels (f–o) reveal the combination of fluorescences originated from LysoTracker and FFSNPs. In panels (f–j), the stained lysosomes are shown with their original blue color which merged to magenta in the overlay with red fluorescing FFSNPs. In order to clarify the overlapping of both colors and to simplify the image analysis for colocalization studies, pseudo micrographs were prepared, in which the lysosomes were shown with pseudo green color allowing the observation of the colocalization with yellow color (panels k–o). Colocalization of fluorescences from LysoTracker and NPs (magenta in panels (f–j) and yellow in panels (k–o)), as indicated by white arrows, clearly demonstrate the intracellular accumulation of FFSNPs inside the endolysosome compartment. Fluorescence from the single red channel denotes FFSNPs in panels (p–t). Analogously, colocalization studies for all FFSNPs (100 μg/mL) were performed in DMEM + AB/AM (1%) and representative results for 6 h incubations are presented in Figure S2, Supporting Information.

Fluorescence microscopy revealed an intracellular presence of all types of FFSNPs investigated in HOBs after exposure to the particles in both serum-free and serum-containing incubation media (Figure 3). As a quantification of particle uptake from such images will not generate reliable data, uptake of FFSNPs after application of 50 and 100 μg/mL into HOB cells was quantified by determining cellular FFSNP fluorescence in a fluorimeter for the cells harvested after the respective

DOI: 10.1021/acsami.5b01900
ACS Appl. Mater. Interfaces 2015, 7, 13821–13833

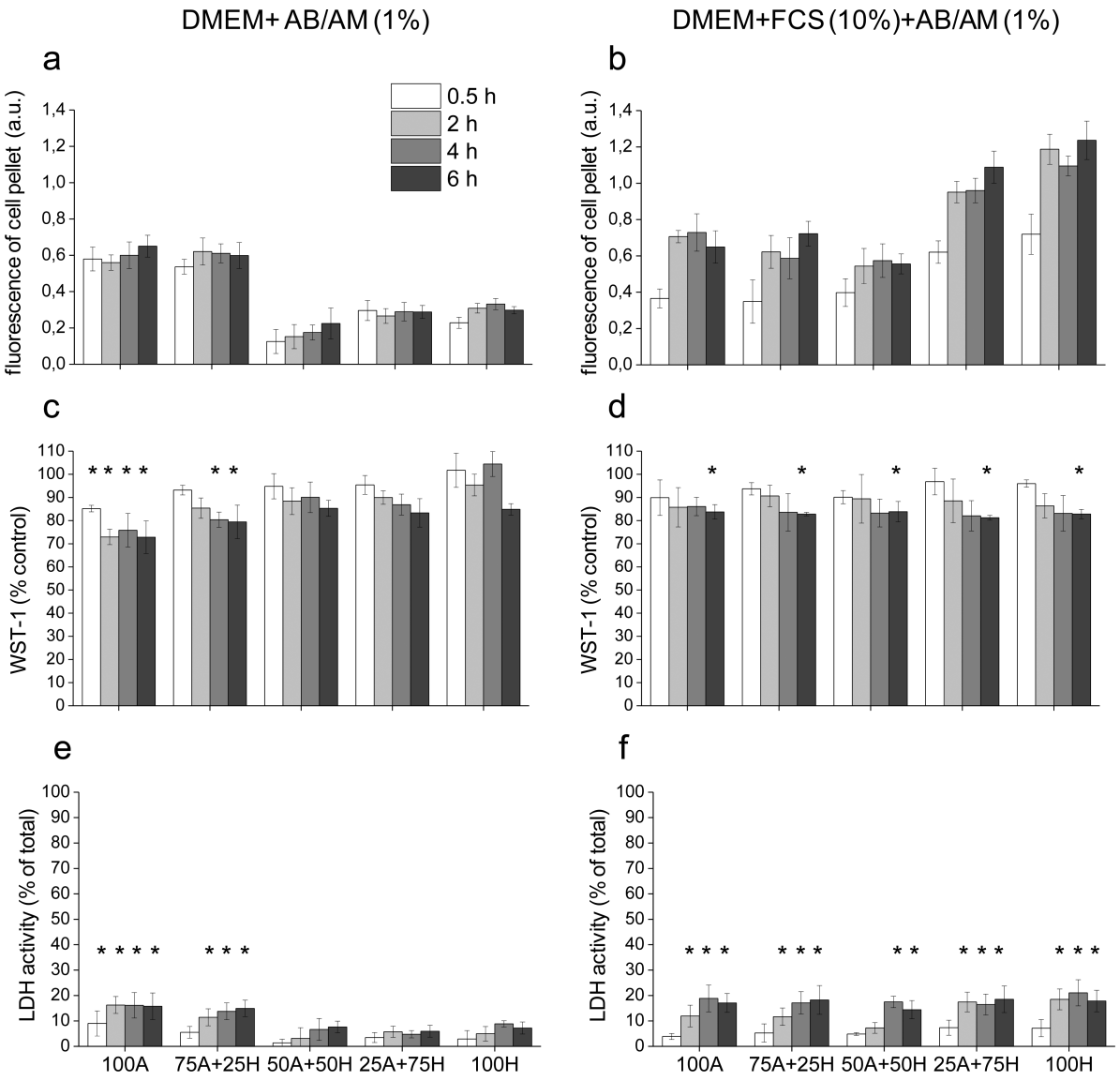

Figure 5. Fluorescence intensity of cellular FFSNPs after incubation of HOB cells with 100 μg/mL of the FFSNPs for the indicated incubation times in serum-free (a) or in serum-supplemented medium (b). Cell viability measured by the WST-1 assay after incubation in medium without (c) or with FCS (d). The data are given as the percentage of the control (cells incubated without NPs). Extracellular LDH activity (given as percent of total LDH in cells and media) released from HOBs after exposure to FFSNPs in serum-free (e) or serum-containing medium (f). All data are expressed as mean ± SD of values obtained in three independent experiments. In (c–f), asterisks (*) indicate significant differences compared to the control ($p < 0.05$).

incubations (Figure S3a,b, Supporting Information, and Figure 5a,b). In serum-free medium, the uptake of positively charged silica NPs (100A and 75A + 25H) was significantly higher than that of anionic and neutral NPs at all four exposure times (Figure S3a, Supporting Information, and Figure 5a). In contrast, higher amounts of cellular fluorescence were observed for cells that had been exposed in the presence of serum to anionic FFSNPs (100H and 25A + 75H) (Figure S3b, Supporting Information, and Figure 5b) compared to the other three types of particles (100A, 75H + 25H and 50A + 50H). Statistical comparison of the results obtained for cells exposed to FFSNPs in the absence or presence of FCS (Figure S3a,b, Supporting Information, and Figure 5a,b) revealed significantly increased ($p < 0.05$) accumulation of the negatively charged (100H and 25A + 75H) and neutral FFSNPs (50A + 50H) in the presence of serum. In contrast, cellular uptake of the positively charged FFSNPs did not differ between incubations in the absence or the presence of serum. In addition, for serum-free conditions, hardly any increase in cellular FFSNP fluorescence was observed between 0.5 and 6 h of incubation, regardless of their surface charge (Figure S3a, Supporting Information, and Figure 5a), while in serum-containing medium the cellular fluorescence was increasing at least between the incubation periods of 0.5 and 2 h (Figure 5b).

The viability of HOB cells after exposure to FFSNPs was assessed using the WST-1 assay and the LDH release. At a concentration of 50 μg/mL, none of the investigated FFSNPs caused any significant loss in cell viability compared to control incubations in media without and with FCS (Figure S3c–f, Supporting Information). However, for some types of FFSNPs, exposure of HOBs to 100 μg/mL of the FFSNPs compromised cell viability to a small but significant level (Figure 5c,d). In the absence of serum, only the cationic FFSNPs, but not the neutral or anionic FFSNPs, lowered the cellular WST-1

DOI: 10.1021/acsami.5b01900
ACS Appl. Mater. Interfaces 2015, 7, 13821–13833

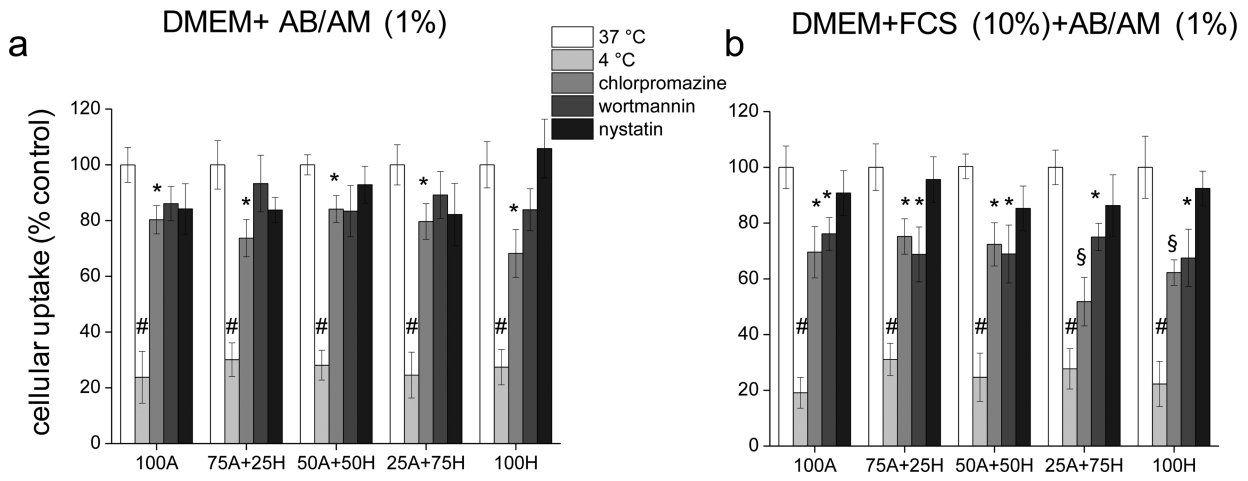

Figure 6. Uptake of FFSNPs (100 μg/mL) into HOB cells after a 2 h exposure at 4 or 37 °C in the absence or at 37 °C in the presence of the endocytosis inhibitors, chlorpromazine (30 μM), wortmannin (300 nM), or nystatin (10 μM) in serum-free (a) or serum-containing medium (b). The amount of cellular particles was quantified by fluorimetry of cell pellets. The data are expressed as means ± SD of three independent experiments and are given as a percentage of the respective FFSNP-treated cells incubated at 37 °C in the presence of the appropriate concentration of DMSO which was used as solvent for the inhibitors. Significant differences between the obtained values and the control are indicated (∗, $p < 0.05$; §, $p < 0.01$; #, $p < 0.001$).

reduction and induced some LDH release (Figure 5c,e). On the contrary, in serum-containing media, all FFSNPs caused a mild but significant loss in WST-1 reduction capacity which was accompanied by an increase in LDH release (Figure 5d,f).

In order to analyze the mechanism of cellular uptake of FFSNPs into HOB, inhibitors of different endocytotic pathways were applied (Figure 6). The inhibitor concentrations used were defined in preliminary experiments and represent the highest concentrations which did not significantly compromise cell viability within a 2 h treatment in both serum-free and serum-containing medium (data not shown). Incubation of HOB cells at 4 °C neither altered WST-1 reduction capacity nor led to higher LDH leakage compared to controls (data not shown) but drastically prevented the cellular accumulation of FFSNPs (Figure 6). In the presence of chlorpromazine, a specific clathrin-mediated endocytosis inhibitor,[38] the cellular uptake of all FFSNPs was lowered in comparison to the respective controls independent of the type of medium applied. However, in the presence of serum, the inhibitory effect of chlorpromazine on cellular uptake was stronger for anionic FFSNP ($p < 0.01$) in comparison to cationic and neutral FFSNPs ($p < 0.05$). When HOB cells were exposed to wortmannin, a macropinocytosis inhibitor,[38] no inhibitory effect on the uptake of FFSNPs was observed in serum-free medium, while the cellular accumulation of FFSNPs was lowered in the presence of wortmannin in serum-containing medium. In contrast, nystatin, an inhibitor of caveolin-dependent endocytosis,[38] did not affect the uptake of FFSNPs (Figure 6).

4. DISCUSSION

4.1. Particle Characterization. The synthesis route of FFSNPs was based on the water in oil reverse microemulsion. First, hydrolysis and condensation of TEOS took place to form fluorescently labeled silica NPs in the presence of the dye RBITS, which was covalently encapsulated in the silica matrix. Second, controlled single- or simultaneous multifunctionalization with amino and/or sulfonate groups was performed. In the applied method, the nanodroplets of water serve as nanoreactors to synthesis the silica NPs and define the final particle size.[32,39] By keeping the concentration of all components including oil, water, surfactant, cosurfactant, precursor, dye, and catalyst constant, this route enabled the synthesis of five types of FFSNPs with identical value for particle size and similar spherical morphology, which differed only regarding the introduced functional groups at the surface (Table 1 and Figure 1a). In addition, by using the same RBITC concentration, particles with similar fluorescence characteristic were obtained as demonstrated by fluorescence spectroscopy and microscopy (Figure 1b).

FFSNPs were systematically characterized by zeta potential measurements and DLS analysis in various media. The zeta potential values determined for water dispersions confirmed that NP surface charge was varied from positive to negative by modulating the concentrations of two surface functionalities in the synthesis (Table 1). The measured zeta potential values of FFSNPs in H_2O correlated to the nature of chemical modification. Particularly, positive zeta potential values were measured for 100A and 75A + 25H due to the dominant presence of amino groups, whereas 100H and 25A + 75 H showed negative surface charge due to the presence of high numbers of sulfonate groups on their surface.

Our results demonstrate that the zeta potential values depended strongly on the composition of the medium, in which FFSNPs dispersions were prepared and measured. While the variation of the FFSNP surface charge was strong in H_2O and DMEM + AB/AM (1%), all FFSNPs acquired similar zeta potentials upon transfer into protein-containing media consistent to other reports.[36,40] In fact, when the NPs were dispersed in H_2O, the zeta potential depended exclusively on the molecular species introduced and their surface properties. In contrast, after dispersions in protein-containing media, cationic and anionic FFSNPs became a net anionic surface charge. This suggests that under these conditions adsorption of proteins and formation of a protein corona takes place, regardless of the initial surface charge of the FFSNPs, as reported previously for a variety of NPs.[21,37,41,42] The zeta potential of FFSNPs determined for protein-containing media is likely to reflect the zeta potential of serum proteins, mainly that of serum albumin.[21,43]

DOI: 10.1021/acsami.5b01900
ACS Appl. Mater. Interfaces 2015, 7, 13821−13833

The amount of adsorbed BSA onto FFSNPs can be correlated to the zeta potential of the particles (Figure 2b). Positively charged FFSNPs adsorbed more BSA compared to the anionic and neutral ones. This observation is in agreement with literature data[35,44] and is consistent with electrostatic interactions as a primary driving force of BSA adsorption onto silica. On the other hand, although the quantification of protein adsorption was carried out in water, in which BSA with an isoelectric point (IEP) of 4.7 features negative charge,[45] protein adsorption was also observed for anionic FFSNPs. This behavior suggests that other forces rather than electrostatic interactions are also involved in the observed BSA adsorption.[35,46]

DLS analysis revealed slow time-dependent aggregation for aqueous dispersions of both cationic and anionic FFSNPs, while almost neutral particle (50A + 50H) aggregated strongly already within 2 h as these NPs have an IEP similar to the pH value of water (Figure 2a). Also for FFSNPs dispersed in serum-free culture medium, rapid aggregation or partial precipitation was observed (Figure 2e). Such a particle aggregation in serum-free medium is most likely caused by the high electrolyte content which reduces the electrostatic repulsion.[47] In addition, immediately after preparation, the D_H of all FFSNPs in protein-containing media was slightly larger than that in pure water (Figure 2c,d,f), which is consistent with the formation of a protein corona around the NPs.[48] Small differences between the colloidal stability of the five investigated FFSNPs in one type of protein-containing medium can be explained by the different initial D_H which depends on the initial surface charge and particularly on the IEP. Depending on the surface charge of FFSNPs, different types of proteins may adsorb[40,49] and/or a different amount of protein may form the corona, as our results from BSA-containing medium suggest (Figure 2b). Besides the type and the amount of proteins adsorbed onto the NPs surface, their conformation depends also on the surface charge.[50] Furthermore, previous studies suggested that the protein corona is highly dynamic with a composition that changes over time due to continuous protein association and dissociation.[20,22]

Compared to protein-free media, the protein corona formed in both FCS- and BSA-containing media prevents the aggregation of silica NPs, regardless of their initial surface charge (Figure 2d,f), consistent with the view that protein corona formation enhances the colloidal stability and prevents aggregation due to steric stabilization.[43,48,51] However, another study reported that the presence of serum proteins induces instability,[52] demonstrating that the aggregation behavior of NPs in cell culture media and its correlation with the formation of a protein corona remains an important issue which has to be separately addressed for each type of NPs and for each experimental cell culture system.

4.2. Cell Culture Experiments. The effect of surface charge-dependent cellular internalization of FFSNPs into HOB cells was studied for serum-free and serum-containing media. Fluorescence microscopy images of the cells after exposure to FFSNPs demonstrated that irrespective of surface charge and composition of medium, all investigated FFSNPs were taken up into the HOB cells and were found to be distributed within the cells as discrete spots (Figure 3). Moreover, colocalization studies with LysoTracker revealed that for all conditions applied FFSNPs were localized in the endolysosomal compartment (Figure 4f–o and Figure S2f–o, Supporting Information), irrespective of the zeta potential of the FFSNPs. This observation suggests that endocytotic processes are involved in the uptake of all investigated types of FFSNPs into HOB cells, consistent with results obtained by other groups on the uptake of silica NPs in different cell lines.[53]

Presence or absence of serum has been reported to strongly affect the uptake and possible toxicity of silica NPs.[53−57,52,58] However, for the conditions used in this study, at best, little impairment of cell viability was observed as determined by two independent viability assays (Figure 5c–f). In serum-free medium, only the cationic FFSNPs compromised to a small extent cell viability but not the neutral or anionic ones which is consistent with a higher amount of internalized NPs observed after exposure to the cationic FFSNPs (Figure 5c,e). In contrast, in serum-containing media, all FFSNPs caused some adverse effects on the cells which did not depend on the level of accumulated NPs (Figure 5d,f). Further studies and other experimental conditions are required to investigate in more detail the toxic potential of the synthesized FFSNPs.

Determining the fluorescence signals originated from internalized FFSNPs in HOB cells allowed one to quantify the uptake of the FFSNPs under various conditions for incubations of up to 6 h. In the absence of serum, the positively charged FFSNPs were accumulated into the HOB cells more strongly than negative ones which was accompanied by a mild toxic effect of the positively charged FFSNPs (Figure S3a, Supporting Information, and Figure 5a). As electrostatic interactions are considered as an important factor to determine NP–cell interaction,[59,60] the stronger accumulation of positive FFSNPs is likely to be initiated by binding to the large negatively charged domains which are present at the cell surface.[61] The observed internalization of negatively charged FFSNPs could involve adsorption to the few cationic sites on the cell surface.[35,59] Cellular uptake of anionic NPs is considered to be less efficient compared to cationic NPs,[62] which was confirmed by our data for serum-free conditions. However, for serum-containing media, we (Figure S3b, Supporting Information, and Figure 5b) and other groups[35,59] demonstrated that anionic NPs are more efficiently accumulated by cells, which is likely to be caused by the presence of a protein corona around the NPs which defines their interactions with cells.[63,19] Anionic and cationic NPs adsorb different proteins from their surrounding medium[64] which will affect their surface properties and thereby also their cellular uptake. For example, the positive zeta potential of FFSNPs supported BSA adsorption (Figure 2b) but led to a lower internalization of the respective NPs by HOB cells (Figure S3b, Supporting Information, and Figure 5b). This is consistent with literature data showing that BSA precoated NPs are taken up less efficiently than uncoated ones.[27]

Protein corona formation has been reported to decrease NP uptake as a consequence of serum presence[57] while other studies contradicted these results and demonstrate increased cellular NP uptake in serum-containing medium.[65] These controversial findings were attributed to different NP properties[21,37] as well as the use of different types of cells.[36] For the conditions and FFSNPs studied here, it can be concluded that the presence of serum proteins enhanced the uptake of negatively charged and neutral FFSNPs, while in the case of cationic FFSNPs hardly any differences were observed for incubations without or with serum. Our results suggest also that differences in colloidal stability of the particles in the absence of serum or an increase in particle size due to corona formation in the presence of serum could contribute to the controversial

DOI: 10.1021/acsami.5b01900
ACS Appl. Mater. Interfaces 2015, 7, 13821−13833

data reported, most likely as both processes increase particle size which is broadly accepted as a determining factor for bionano interactions.[66]

Microscopic images as well as the quantification of cellular fluorescence of FFSNP-treated HOB cells revealed that already large amounts of fluorescent particles had been taken up within 30 min. During longer incubation times, no further accumulation of NPs was observed in serum-free medium while in the presence of serum almost maximal amounts of cellular FFSNPs were observed after 2 h of incubation. A possible reason for this observation could be that the high tendency of FFSNPs to aggregate in serum-free medium could drastically decrease the efficiency of HOB cells for internalization of such particles over time. Alternatively, different mechanisms for cellular binding and uptake of anionic and cationic NPs in the presence and absence of serum may contribute to the observed outcomes.[23] For all FFSNPs, temperature-dependent uptake into HOB cells was observed by quantitative analysis of cellular FFSNPs (Figure 6) and by fluorescence microscopy (data not shown), which revealed that hardly any particle had been accumulated at 4 °C in the cells. This drastic inhibition of FFSNPs uptake into HOB cells at 4 °C is most likely attributed to the impairment of cellular energy metabolism, which diminishes energy-dependent endocytosis.[67,68]

Indeed, endocytosis appears to be involved in the uptake of FFSNPs into HOB cells. At least chlorpromazine, which is an inhibitor of clathrin-mediated endocytosis,[38] significantly lowered FFSNP accumulation in both the absence or the presence of serum, which is consistent with literature data on the clathrin-dependent uptake of silica particles into human mesenchymal stem cells.[69,70] In serum-containing medium, the uptake of FFSNPs was also lowered by the macropinocytosis inhibitor wortmannin,[38] suggesting that in HOB cells in the presence of serum both clathrin-dependent endocytosis and macropinocytosis contribute to FFSNP uptake. In contrast, caveolin-dependent processes appear not to be involved as nystatin, an inhibitor of such endocytotic processes,[38] did not affect FFSNP accumulation. Under the conditions used, none of the applied inhibitors was able to completely prevent FFSNP accumulation, suggesting that other mechanisms are involved in the internalization of FFSNPs into HOB cells. Further studies are needed to address in more detail the cellular uptake and the potential involvement of endocytotic pathways in the cellular internalization of silica particles with different types of surface charge.

5. CONCLUSION

Fluorescent silica NPs with a narrow size distribution were prepared and single or multifunctionalized by introducing amino and sulfonate groups, allowing the successful adjustment of the zeta potential from highly positive to highly negative, while other properties of the NPs were kept almost constant. The protein corona formed around FFSNPs upon transfer into protein-containing media neutralizes the zeta potential values and stabilizes the particles against agglomeration.

Our results underline the importance and relevant role of the surface charge of NPs and the composition of the medium for interactions of NPs with cells. HOB cells internalized anionic and cationic silica NPs with opposite trends in serum-free and serum-containing cell culture media. A positive surface charge of silica NPs was favorable for uptake by osteoblasts in the absence of serum, while in serum-supplemented medium as a consequence of protein corona formation, anionic silica NPs were internalized by HOB cells with higher efficiency. Different endocytosis pathways may be responsible for the differences observed for the accumulation of silica NPs in the absence or presence of serum. The results shown confirm that surface functionalization of silica NPs can be successfully exploited to control cellular interactions and NP uptake. Our results suggest that, for physiological conditions in the presence of serum proteins, sulfonate dominant functionalized silica NP should be applied to achieve a high level of cellular uptake. In contrast, for application of silica NPs to cells for mechanistic studies in serum-free conditions in vitro as well as for direct tissue applications in vivo, which avoid contact of silica NP to blood and serum proteins, accelerated cellular uptake could be expected for amino-functionalized NPs. We anticipate that the results of our in vitro experiments using FFSNPs are of interest for future studies aimed to optimize the design of NPs to better control cellular uptake and cell responses.

■ ASSOCIATED CONTENT

Supporting Information

Size distribution, colocalization of FFSNPs with lysosomes, and fluorescence intensity of HOB cell pellet after association with FFSNPs. The Supporting Information is available free of charge on the ACS Publications website at DOI: 10.1021/acsami.5b01900.

■ AUTHOR INFORMATION

Corresponding Author

*E-mail: treccani@uni-bremen.de. Tel: +49 421 218 64938. Fax: +49 421 218 64932.

Notes

The authors declare no competing financial interest.

■ ACKNOWLEDGMENTS

We greatly thank Dr. Florian Schlüter (Advanced Ceramics, University Bremen) for measurements of gas adsorption, Dr. Thorsten Mehrtenz (Solid State Physics, University Bremen) for STEM analysis, and Dr. Jan Köser (Zentrale Analytik, University Bremen) for the support for DLS measurements. This work was supported by the European Research Council within the SIRG Project "BiocerEng" Project No. 205509.

■ REFERENCES

(1) Hornig, S.; Biskup, C.; Gräfe, A.; Wotschadlo, J.; Liebert, T.; Mohr, G.; Heinze, T. Biocompatible Fluorescent Nanoparticles for pH-Sensoring. *Soft Matter* **2008**, *4*, 1169−1172.

(2) Latterini, L.; Amelia, M. Sensing Proteins with Luminescent Silica Nanoparticles. *Langmuir* **2009**, *25*, 4767−4773.

(3) Liong, M.; Lu, J.; Kovochich, M.; Xia, T.; Ruehm, S.; Nel, A.; Tamanoi, F.; Zink, J. Multifunctional Inorganic Nanoparticles for Imaging, Targeting, and Drug Delivery. *ACS Nano* **2008**, *2*, 889−896.

(4) Kumar, R.; Roy, I.; Ohulchanskyy, T.; Goswami, L.; Bonoiu, A.; Bergey, E.; Tramposch, K.; Maitra, A.; Prasad, P. Covalently Dye-Linked, Surface-Controlled, and Bioconjugated Organically Modified Silica Nanoparticles as Targeted Probes for Optical Imaging. *ACS Nano* **2008**, *2*, 449−456.

(5) Rosenholm, J.; Sahlgren, C.; Lindén, M. Towards Multifunctional, Targeted Drug Delivery Systems Using Mesoporous Silica Nanoparticles − Opportunities & Challenges. *Nanoscale* **2010**, *2*, 1870−1883.

(6) Febvay, S.; Marini, D.; Belcher, A.; Clapham, D. Targeted Cytosolic Delivery of Cell-Impermeable Compounds by Nanoparticle-

DOI: 10.1021/acsami.5b01900
ACS Appl. Mater. Interfaces 2015, 7, 13821−13833

Mediated, Light-Triggered Endosome Disruption. *Nano Lett.* **2010**, *10*, 2211−2219.
(7) Fuller, J.; Zugates, G.; Ferreira, L.; Ow, H.; Nguyen, N.; Wiesner, U.; Langer, R. Intracellular Delivery of Coreeshell Fluorescent Silica Nanoparticles. *Biomaterials* **2008**, *29*, 1526−1532.
(8) Xia, T.; Kovochich, M.; Liong, M.; Meng, H.; Kabehie, S.; George, S.; Zink, J.; Nel, A. Polyethyleneimine Coating Enhances the Cellular Uptake of Mesoporous Silica Nanoparticles and Allows Safe Delivery of siRNA and DNA Constructs. *ACS Nano* **2009**, *3*, 3273−3286.
(9) Jia, T.-t.; Cai, Z.-m.; Chen, X.-m.; Lin, Z.-j.; Huang, X.-l.; Chen, X.; Chen, G.-n. Electrogenerated Chemiluminescence Ethanol Biosensor Based on Alcohol Dehydrogenase Functionalized Ru(bpy)-32+ Dodoped Silica Nanoparticles. *Biosens. Bioelectron.* **2009**, *25*, 263−267.
(10) Gao, X.; He, J.; Deng, L.; Cao, H. Synthesis and Characterization of Functionalized Rhodamine B-Doped Silica Nanoparticles. *Opt. Mater.* **2009**, *31*, 1715−1719.
(11) Peng, J.; He, X.; Wang, K.; Tan, W.; Wang, Y.; Y, L. Noninvasive Monitoring of Intracellular pH Change Induced by Drug Stimulation Using Silica Nanoparticle Sensors. *Anal. Bioanal. Chem.* **2007**, *388*, 645−654.
(12) Kumar, R.; Roy, I.; Ohulchanskky, T.; Vathy, L.; Bergey, E.; Sajjad, M.; Prasad, P. In Vivo Biodistribution and Clearance Studies Using Multimodal Organically Modified Silica Nanoparticles. *ACS Nano* **2010**, *4*, 699−708.
(13) Labéguerie-Egeá, J.; McEvoy, H.; McDonagh, C. Synthesis, Characterisation and Functionalisation of Luminescent Silica Nanoparticles. *J. Nanopart. Res.* **2011**, *13*, 6455−6465.
(14) Santra, S.; Zhang, P.; Wang, K.; Tapec, R.; Tan, W. Conjugation of Biomolecules with Luminophore-Doped Silica Nanoparticles for Photostable Biomarkers. *Anal. Chem.* **2001**, *73*, 4988−4993.
(15) Lee, J.; Jun, Y.; Yeon, S.; Shin, J.; Cheon, J. Dual-Mode Nanoparticle Probes for High-Performance Magnetic Resonance and Fluorescence Imaging of Neuroblastoma. *Angew. Chem.* **2006**, *118*, 8340−8342.
(16) Salvati, A.; Pitek, A.; Monopoli, M.; Prapainop, K.; Bombelli, F.; Hristov, D.; Kelly, P.; Åberg, C.; Mahon, E.; Dawson, K. Transferrin-Functionalized Nanoparticles Lose Their Targeting Capabilities When a Biomolecule Corona Adsorbs on the Surface. *Nat. Nanotechnol.* **2013**, *8*, 137−143.
(17) Mahon, E.; Salvati, A.; Bombelli, F.; Lynch, I.; Dawson, K. Designing the Nanoparticle−Biomolecule Interface for "Targeting and Therapeutic Delivery". *J. Controlled Release* **2012**, *161*, 164−174.
(18) Mahmoudi, M.; Lynch, I.; Ejtehadi, M.; Monopoli, M.; Bombelli, F.; Laurent, S. Protein Nanoparticle Interactions: Opportunities and Challenges. *Chem. Rev.* **2011**, *111*, 5610−5637.
(19) Nel, A.; Mädler, L.; Velegol, D.; Xia, T.; Hoek, E.; Somasundaran, P.; Klaessig, F.; Castranova, V.; Thompson, M. Understanding Biophysicochemical Interactions at the Nano−Bio Interface. *Nat. Mater.* **2009**, *8*, 543−557.
(20) Monopoli, M.; Åberg, C.; Salvati, A.; Dawson, K. Biomolecular Coronas Provide the Biological Identity of Nanosized Materials. *Nat. Nanotechnol.* **2012**, *7*, 779−786.
(21) Fleischer, C.; Payne, C. Nanoparticle Surface Charge Mediates the Cellular Receptors Used by Protein−Nanoparticle Complexes. *J. Phys. Chem. B* **2012**, *116*, 8901−8907.
(22) Casals, E.; Pfaller, T.; Duschl, A.; Oostingh, G. J.; Puntes, V. Time Evolution of the Nanoparticle Protein Corona. *ACS Nano* **2010**, *4*, 3623−3632.
(23) Fleischer, C.; Payne, C. Nanoparticle−Cell Interactions: Molecular Structure of the Protein Corona and Cellular Outcomes. *Acc. Chem. Res.* **2014**, *47*, 2651−2659.
(24) Lundqvist, M.; Stigler, J.; Elia, G.; Lynch, I.; Cedervall, T.; Dawson, K. Nanoparticle Size and Surface Properties Determine the Protein Corona with Possible Implications for Biological Impacts. *Proc. Natl. Acad. Sci. U.S.A.* **2008**, *105*, 14265−14270.
(25) Kettiger, H.; Schipanski, A.; Wick, P.; Huwyler, J. Engineered Nanomaterial Uptake and Tissue Distribution: from Cell to Organism. *Int. J. Nanomed.* **2013**, *8*, 3255−3269.
(26) Aggarwal, P.; Hall, J.; McLeland, C.; Dobrovolskaia, M.; McNeil, S. Nanoparticle Interaction with Plasma Proteins as It Relates to Particle Biodistribution, Biocompatibility and Therapeutic Efficacy. *Adv. Drug Delivery Rev.* **2009**, *61*, 428−437.
(27) Baier, G.; Costa, C.; Zeller, A.; Baumann, D.; Sayer, C.; Araujo, P.; Mailänder, V.; Musyanovych, A.; Landfester, K. BSA Adsorption on Differently Charged Polystyrene Nanoparticles Using Isothermal Titration Calorimetry and the Influence on Cellular Uptake. *Macromol. Biosci.* **2011**, *11*, 628−638.
(28) Kim, B.; Han, G.; Toley, B.; Kim, C.; Rotello, V.; Forbes, N. Tuning Payload Delivery in Tumour Cylindroids Using Gold Nanoparticles. *Nat. Nanotechnol.* **2010**, *5*, 465−472.
(29) Harris, T.; Green, J.; Fung, P.; Langer, R.; Anderson, D.; Bhatia, S. Tissue-Specific Gene Delivery via Nanoparticle Coating. *Biomaterials* **2010**, *31*, 998−1006.
(30) Schaeublin, N.; Braydich-Stolle, L.; Schrand, A.; Miller, J.; Hutchison, J.; Schlager, J.; Hussain, S. Surface Charge of Gold Nanoparticles Mediates Mechanism of Toxicity. *Nanoscale* **2011**, *3*, 410−420.
(31) Asati, A.; Santra, S.; Kaittanis, C.; Perez, J. Surface-Charge-Dependent Cell Localization and Cytotoxicity of Cerium Oxide Nanoparticles. *ACS Nano* **2010**, *4*, 5321−5331.
(32) Bagwe, R.; Yang, C.; Hilliard, L.; Tan, W. Optimization of Dye-Doped Silica Nanoparticles Prepared Using a Reverse Microemulsion Method. *Langmuir* **2004**, *20*, 8336−8342.
(33) Brunauer, S.; Emmett, P.; Teller, E. Adsorption of Gases in Multimolecular Layers. *J. Am. Chem. Soc.* **1938**, *60*, 309−319.
(34) Holthaus, M.; Stolle, J.; Treccani, L.; Rezwan, K. Orientation of Human Osteoblasts on Hydroxyapatite-Based Microchannels. *Acta Biomater.* **2012**, *8*, 394−403.
(35) Patil, S.; Sandberg, A.; Heckert, E.; Self, W.; Seal, S. Protein Adsorption and Cellular Uptake of Cerium Oxide Nanoparticles as a Function of Zeta Potential. *Biomaterials* **2007**, *28*, 4600−4607.
(36) Yan, Y.; Gause, K.; Kamphuis, M.; Ang, C.; O'Brien-Simpson, N.; Lenzo, J.; Reynolds, E.; Nice, E.; Caruso, F. Differential Roles of the Protein Coronain the Cellular Uptake of Nanoporous Polymer Particles by Monocyte and Macrophage Cell Lines. *ACS Nano* **2013**, *7*, 10960−10970.
(37) Fleischer, C.; Kumar, U.; Payne, C. Cellular Binding of Anionic Nanoparticles Is Inhibited by Serum Proteins Independent of Nanoparticle Composition. *Biomater. Sci.* **2013**, *1*, 975−982.
(38) Khalil, I.; Kogure, K.; Akita, H.; Harashima, H. Uptake Pathways and Subsequent Intracellular Trafficking in Nonviral Gene Delivery. *Pharmacol. Rev.* **2006**, *58*, 32−45.
(39) Nooney, R.; McCahey, C.; Stranik, O.; Guevel, X.; McDonagh, C.; MacCraith, B. Experimental and Theoretical Studies of the Optimisation of Fluorescence from Near-Infrared Dye-Doped Silica Nanoparticles. *Anal. Bioanal. Chem.* **2009**, *393*, 1143−1149.
(40) Guarnieri, D.; Malvindi, M.; Belli, V.; Pompa, P.; Netti, P. Effect of Silica Nanoparticles with Variable Size and Surface Functionalization on Human Endothelial Cell Viability and Angiogenic Activity. *J. Nanopart. Res.* **2014**, *16*, 1−14.
(41) Lindman, S.; Lynch, I.; Thulin, E.; Nilsson, H.; Dawson, K.; Linse, S. Systematic Investigation of the Thermodynamics of HSA Adsorption to *N*-iso-Propylacrylamide/*N*-tert-Butylacrylamide Copolymer Nanoparticles. Effects of Particle Size and Hydrophobicity. *Nano Lett.* **2007**, *7*, 914−920.
(42) Izak-Nau, E.; Voetz, M.; Eiden, S.; Duschl, A.; Puntes, V. F. Altered Characteristics of Silica Nanoparticles in Bovine and Human Serum: The Importance of Nanomaterial Characterization Prior to Its Toxicological Evaluation. *Part. Fibre Toxicol.* **2013**, *10*, 1−12.
(43) Horie, M.; Kato, H.; Iwahashi, H. Cellular Effects of Manufactured Nanoparticles: Effect of Adsorption Ability of Nanoparticles. *Arch. Toxicol.* **2013**, *87*, 771−781.
(44) Rezwan, K.; Meier, L.; Gauckler, L. Lysozyme and Bovine Serum Albumin Adsorption on Uncoated Silica and AlOOH-Coated

DOI: 10.1021/acsami.5b01900
ACS Appl. Mater. Interfaces 2015, 7, 13821−13833

Silica Particles: The Influence of Positively and Negatively Charged Oxide Surface Coatings. *Biomaterials* **2005**, *26*, 4351−4357.
(45) Chun, K.-Y.; Stroeve, P. Protein Transport in Nanoporous Membranes Modified with Self-Assembled Monolayers of Functionalized Thiols. *Langmuir* **2002**, *18*, 4653−4658.
(46) Robertson, B.; Zyndey, A. Protein Adsorption in Asymmetric Ultrafiltration Membranes with Highly Constricted Pores. *J. Colloid Interface Sci.* **1990**, *134*, 563−575.
(47) Jiang, J.; Oberdörster, G.; Biswas, P. Characterization of Size, Surface Charge, and Agglomeration State of Nanoparticle Dispersions for Toxicological Studies. *Nanopart. Res.* **2009**, *11*, 77−89.
(48) Mahl, D.; Greulich, C.; Meyer-Zaika, W.; Köller, M.; Epple, M. Gold Nanoparticles: Dispersibility in Biological Media and Cell-Biological Effect. *J. Mater. Chem.* **2010**, *20*, 6176−6181.
(49) Graf, C.; Gao, Q.; Schütz, I.; Noufele, C.; Ruan, W.; Posselt, U.; Korotianskiy, E.; Nordmeyer, D.; Rancan, F.; Hadam, S.; Vogt, A.; Lademann, J.; Haucke, V.; Rühl, E. Surface Functionalization of Silica Nanoparticles Supports Colloidal Stability in Physiological Media and Facilitates Internalization in Cells. *Langmuir* **2012**, *28*, 7598−7613.
(50) Keselowsky, B.; Collard, D.; García, A. Surface Chemistry Modulates Fibronectin Conformation and Directs Integrin Binding and Specificity to Control Cell Adhesion. *J. Biomed. Mater. Res., Part A* **2003**, *66A*, 247−259.
(51) Gebauer, J.; Malissek, M.; Simon, S.; Knauer, S.; Maskos, M.; Stauber, R.; Peukert, W.; Treuel, L. Impact of the Nanoparticle−Protein Corona on Colloidal Stability and Protein Structure. *Langmuir* **2012**, *28*, 9673−9679.
(52) Díaz, B.; Sánchez-Espinel, C.; Arruebo, M.; Faro, J.; de Miguel, E.; Magadán, S.; Yagüe, C.; Fernández-Pacheco, R.; Ibarra, M.; Santamaría, J.; González-Fernández, A. Assessing Methods for Blood Cell Cytotoxic Responses to Inorganic Nanoparticles and Nanoparticle Aggregates. *Small* **2008**, *4*, 2025−2034.
(53) Al-Rawi, M.; Diabate´, S.; Weiss, C. Uptake and Intracellular Localization of Submicron and Nano-Sized SiO_2 Particles in HeLa Cells. *Arch. Toxicol.* **2011**, *85*, 813−826.
(54) Kittler, K.; Greulich, C.; Gebauer, J.; Diendorf, J.; Treuel, L.; Ruiz, L.; Gonzalez-Calbet, J.; Vallet-Regi, M.; Zellner, R.; Köller, M.; Epple, M. The Influence of Proteins on the Dispersability and Cell-Biological Activity of Silver Nanoparticles. *J. Mater. Chem.* **2010**, *20*, 512−518.
(55) Panas, A.; Marquardt, C.; Nalcaci, O.; Bockhorn, H.; Baumann, W.; Paur, H.-R.; Mülhopt, S.; Diabaté, S.; Weiss, C. Screening of Different Metal Oxide Nanoparticles Reveals Selective Toxicity and Inflammatory Potential of Silica Nanoparticles in Lung Epithelial Cells and Macrophages. *Nanotoxicology* **2012**, 1−15.
(56) Rancan, F.; Gao, Q.; Graf, C.; Troppens, S.; Hadam, S.; Hackbarth, S.; Kembuan, C.; Blume-Peytavi, U.; Rühl, E.; Lademann, J.; Vogt, A. Skin Penetration and Cellular Uptake of Amorphous Silica Nanoparticles with Variable Size, Surface Functionalization, and Colloidal Stability. *ACS Nano* **2012**, *6*, 6829−6842.
(57) Lesniak, A.; Fenaroli, F.; Monopoli, M.; Åberg, C.; Dawson, K.; Salvati, A. Effects of the Presence or Absence of a Protein Corona on Silica Nanoparticle Uptake and Impact on Cells. *ACS Nano* **2012**, *6*, 5845−5857.
(58) Kim, J.; Salvati, A.; Åberg, C.; Dawson, K. A. Suppression of Nanoparticle Cytotoxicity Approaching in Vivo Serum Concentrations: Limitations of in Vitro Testing for Nanosafety. *Nanoscale* **2014**, *6*, 14180−14184.
(59) Wilhelm, C.; Billotey, C.; Roger, J.; Pons, J.; Bacri, J.; Gazeau, F. Intracellular Uptake of Anionic Superparamagnetic Nanoparticles as a Function of their Surface Coating. *Biomaterials* **2003**, *24*, 1001−1011.
(60) Lorenz, M.; Holzapfel, V.; Musyanovych, A.; Nothelfer, K.; Walther, P.; Frank, H.; Landfester, K.; Schrezenmeier, H.; Mailänder, V. Uptake of Functionalized, Fluorescent-Labeled Polymeric Particles in Different Cell Lines and Stem Cells. *Biomaterials* **2006**, *27*, 2820−2828.
(61) Mahmoudi, M.; Meng, J.; Xue, X.; Liang, C.; Rahmand, M.; Pfeiffer, C.; Hartmann, R.; Gil, P.; Pelaz, B.; Parak, W.; del Pino, P.; Carregal-Romero, S.; Kanaras, A.; Selvan, S. Interaction of Stable Colloidal Nanoparticles with Cellular Membranes. *Biotechnol. Adv.* **2014**, 1−14.
(62) Verma, A.; Stellacci, F. Effect of Surface Properties on Nanoparticle−Cell Interactions. *Small* **2010**, *6*, 12−21.
(63) Tenzer, S.; Docter, D.; Kuharev, J.; Musyanovych, A.; Fetz, V.; Hecht, R.; Schlenk, F.; Fischer, D.; Kiouptsi, K.; Reinhardt, C.; Landfester, K.; Schild, H.; Maskos, M.; Knauer, S.; Stauber, R. Rapid Formation of Plasma Protein Corona Critically Affects Nanoparticle Pathophysiology. *Nat. Nanotechnol.* **2013**, *8*, 772−781.
(64) Fröhlich, E. The Role of Surface Charge in Cellular Uptake and Cytotoxicity of Medical Nanoparticles. *Int. J. Nanomed.* **2012**, *7*, 5577−5591.
(65) Ryman-Rasmussen, J.; Riviere, J.; Monteiro-Riviere, N. Variables Influencing Interactions of Untargeted Quantum Dot Nanoparticles with Skin Cells and Identification of Biochemical Modulators. *Nano Lett.* **2007**, *7*, 1344−1348.
(66) Albanese, A.; Tang, P.; Chan, W. The Eeffect of Nanoparticle Size, Shape, and Surface Chemistry on Biological Systems. *Annu. Rev. Biomed. Eng.* **2012**, *14*, 1−16.
(67) Lu, J.; Liong, M.; Sherman, S.; Xia, T.; Kovochich, M.; Nel, A.; Zink, J.; Tamanoi, F. Mesoporous Silica Nanoparticles for Cancer Therapy: Energy-Dependent Cellular Uptake and Delivery of Paclitaxel to Cancer Cells. *Nanobiotechnology* **2007**, *3*, 89−95.
(68) Dausend, J.; Musyanovych, A.; Dass, M.; Walther, P.; Schrezenmeier, H.; Landfester, K.; Mailänder, V. Uptake Mechanism of Oppositely Charged Fluorescent Nanoparticles in HeLa Cells. *Macromol. Biosci.* **2008**, *8*, 1135−1143.
(69) Huang, D.; Hung, Y.; Ko, B.; Hsu, S.; Chen, W.; Chien, C.; Tsai, C.; Kuo, C.; Kang, J.; Yang, C.; Mou, C.; Chen, Y. Highly Efficient Cellular Labeling of Mesoporous Nanoparticles in Human Mesenchymal Stem Cells: Implication for Stem Cell Tracking. *FASEB J.* **2005**, *19*, 2014−2016.
(70) Chung, T.; Wu, S.; Yao, M.; Lu, C.; Lin, Y.; Hung, Y.; Mou, C.; Chen, Y.; Huang, D. The Effect of Surface Charge on the Uptake and Biological Function of Mesoporous Silica Nanoparticles in 3T3-L1 Cells and Human Mesenchymal Stem Cells. *Biomaterials* **2007**, *28*, 2959−2966.

DOI: 10.1021/acsami.5b01900
ACS Appl. Mater. Interfaces 2015, 7, 13821−13833